An Electron Microscopy Study of Sintering in Three Dental Porcelains

Alexander J. G. Lunt*, Tee K. Neo, and Alexander M. Korsunsky

Abstract— **In the manufacture of yttria partially stabilised zirconia dental prostheses, layers of porcelain veneer are sintered onto zirconia copings in order to reduce surface hardness and to produce an aesthetically pleasing finish. The stress of this interfacial bond and of the near-interface porcelain layers is crucial for reducing the likelihood of chipping during use. An improved understanding of the sintering behavior and the resulting microstructure is therefore required to ensure good prosthesis performance.**

In this study we use scanning electron microscopy in combination with energy dispersive spectroscopy mapping to examine the impact of vacuum sintering on the microstructure and elemental distribution of three types IPS e.max® Ceram dental porcelain (Incisal, B1 shade and C4 shade) over $400 \times 400 \, \mu m^2$ regions. It was found that the powder samples showed distinct differences in the average grain size ($7 - 16 \, \mu m$), maximum grain size ($12 - 33 \, \mu m$) and elemental composition prior to sintering.

Following the application of the recommended sintering regimes, clear differences could be observed between the three samples. The Incisal porcelain demonstrated a uniform surface with limited numbers of grains and no evidence for porosity. In contrast, large numbers of sodium, aluminum and calcium rich grains were observed on the surface of the shaded porcelains, along with clear evidence of voiding.

Index Terms— **Dental porcelain, energy dispersive spectroscopy, scanning electron microscopy, yttria partially stabilised zirconia and sintering.**

I. INTRODUCTION

YTTRIA Partially Stabilized Zirconia (YPSZ) ceramics have, in recent years, become increasingly used as the coping material in the manufacture of dental prostheses [1]. The high strength, high toughness, chemical inertness, biocompatibility and appearance of this material has enabled more reliable and aesthetically pleasing dental implants to be produced [2].

During manufacture, YPSZ copings are veneered with porcelain in order to produce a translucent surface similar to those of real teeth and to prevent wear of existing teeth

through reduced surface hardness [3]. This veneering procedure is a manual multi-stage approach which involves incrementally sintering layers of porcelain onto the coping in order to build up the completed prosthesis. During this process, porcelains of different composition are selected to create different shades and to control the porcelain characteristics within the prosthesis. Despite the benefits associated with this method, this approach has been shown to be linked to the primary failure mode of YPSZ-porcelain prostheses - near interface chipping of porcelain veneer [4].

Analysis of the near-interface region has demonstrated that the origin of the failures is a complex interaction between temperature, microstructure, material characteristics and residual stress which is induced during the sintering process [5, 6]. Much focus has therefore been directed towards improving current understanding of the influence of sintering on the resulting porcelain. For example, different slurry preparation techniques have been shown to induce changes in porcelain microstructure and strength [7]. Incomplete sintering has also been shown to induce porosity in the porcelain [8, 9] and thereby reduce expected prosthesis lifetimes [10].

Despite the insight offered by these studies, an improved understanding of the impact of sintering is necessary to further reduce the prosthesis failures. For this reason the combination of Scanning Electron Microscopy (SEM) and Energy Dispersive Spectroscopy (EDS) was used to study three types of porcelain before and after a single sintering cycle. It is hoped that the combination of these two high resolution techniques will provide insight into the sintering process and its influence on the microstructure and elemental diffusion in porcelain.

II. EXPERIMENTAL

A. Sample Preparation

The three types of porcelain selected for further examination in this study were IPS e.max® Ceram powder based ceramics, which are manufactured by Ivoclar Vivadent. The Incisal (I) porcelain selected is an unshaded porcelain which is designed to have similar fluorescence and opalescence to natural enamel. The other two porcelain types were chosen to be shaded porcelains of type B1 and C4 which are used to match the completed prosthesis shade to that of patients existing teeth.

Powder samples of each of the three types of porcelain were prepared on carbon tabs mounted onto SEM stubs. In order to generate a uniform surface of material, the adhesive surface of the each tab was placed 'face-down' into a petri-dish containing a small amount the porcelain powder. The manual application of a small amount of force to the stub resulted in a moderate amount of compacted material being

collected, which could then be transferred to the SEM for imaging. Mounting the sample in this way ensured a minimal conductive path between the carbon tab and porcelain which minimized the effect of charging on the EDS and SEM imaging which followed.

In order to be as representative as possible of the sintering observed during prosthesis manufacture, 10 mm diameter YPSZ discs were selected as the coping material onto which the three porcelains were veneered. The veneering process outlined in the IPS "Instructions for Use" [11] was implemented for each of the samples to ensure that the results were as characteristic as possible.

Deionized water was applied to a small amount of each type of porcelain and a paintbrush was then used to mix these two constituents together manually. Excess water was removed from the solution using a paper towel, in order to leave a viscous, creamy porcelain slurry. This slurry was manually applied to the surface of the YPSZ at a thickness of approximately $1-2$ mm as per the manufacturer's instructions.

For each of the different porcelain types the manufacturer's recommended sintering regimes [11] were implemented using the Ivoclar Vivadent, Programat P310 vacuum furnace at the Multi Beam Laboratory for Engineering Microscopy (MBLEM), Oxford, UK. The heating, furnace cooling, and atmospheric cooling durations were carefully controlled by the automated furnace in order to meet the exacting requirements from the manufacturer.

In order to reduce the impact of charging, the porcelain samples were mounted onto SEM stubs using carbon tabs. The Mini Sputter Coater SC7620 (Quorum Technologies, UK) at the Laboratory for In-situ Microscopy and Analysis (LIMA), Oxford, UK was then used to apply a 5 nm coat of Au/Pd to the surface of the samples in order to improve conductivity further.

B. Scanning Electron Microscopy

SEM imaging of each of the powdered and sintered samples was performed using Tescan Lyra 3XM FIB-SEM at MBLEM, Oxford, UK. Despite the attempts to reduce the impact of charging, the underlying poor conductivity required very careful optimisation of the imaging parameters. The combination of accelerating voltage of 30 kV and probe current of 190 mA were found to be optimal for imaging the 400 µm viewfield. Images of size 2048×2048 pixels were captured and a dwell time of 1.1µs/pixel was chosen as a compromise between reducing the impact of noise, on the one hand, and to avoid the increased impact of charging associated with longer dwells, on the other.

C. Energy Dispersive Spectroscopy

In order to quantify the elemental weight percentage distribution in each of the imaging locations, the X-Max Silicon Drift detector (Oxford Instruments, UK) at MBLEM was used to perform EDS analysis. In order to maintain consistency, the optimized SEM conditions were maintained throughout the analysis. The only parameter that was changed was the incident beam intensity, which was optimized in order to minimize the 'dead time' of the EDS detector. This value was found to vary between $12-14$ a. u. depending upon the exact sample being imaged.

EDS maps of size 2048×2048 pixels were captured using the software AZtecEnergy from Oxford Instruments.

A dwell time of 100 µs/pixel was found to be sufficient to reduce the impact of noise on the resulting maps to insignificant levels and 'Quantmap' tool was used to improve further the quality of the elemental weight percent images produced.

III. RESULTS

A. Scanning Electron Microscopy

The SEM images of the powdered and sintered porcelain samples are shown in Fig. 1. Visual examination of the three powdered compositions revealed that despite the limited size of the images captured, distinct variations in both the average and maximum grain sizes were observed. For this reason grain size analysis was performed using the automated thresholding and particle identification routine 'Analyze Particles' in the image processing software ImageJ [12]. Several hundreds of grains were identified in each image and the average and maximum grain size for the three powders is shown in Table I. The minimum grain sizes were found to be limited solely by the resolution of the images captured and therefore were not included for direct comparison.

Despite the limited size of the images examined in this study, the quantitative grain size distributions identified show clear differences between the three porcelain types. The average grain size in the Incisal material was found to be approximately 2.3 times larger than in the C4 porcelain and 1.1 times larger than the B1 porcelain. In contrast to this trend, the largest particle was observed in B1, which was found to be 1.1 times larger than the Incisal porcelain and 2.8 times larger than C4. These differences demonstrate that the morphology and size distribution of the three porcelain powders were distinct prior to the sintering process.

Critical analysis of the sintered specimens also revealed distinct variations between the three completed veneers. On each of the completed surfaces a range of particles of varying size were observed. For this reason a similar particle identification analysis was performed using ImageJ [12], and the results of this study are shown in Table II.

In the sintered samples, regions of voiding were also observed in both of the shaded porcelains. Attempts were made to quantify the distribution of this voiding behavior using the same automated particle identification routine,
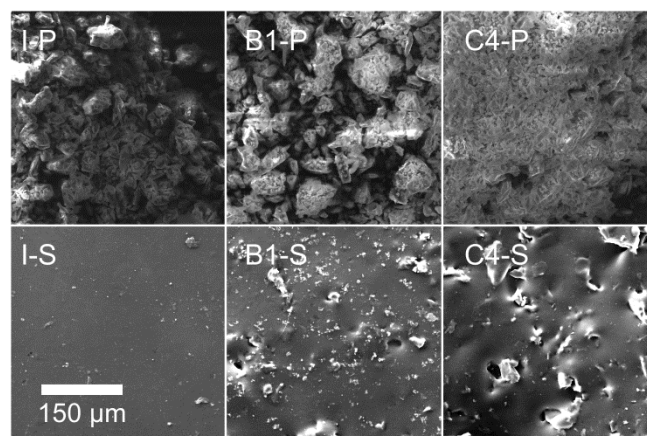

Fig. 1. SEM images of the Incisal (I), B1 and C4 porcelain compounds. The powder (P) and sintered (S) versions are shown to demonstrate the impact of sintering on the microstructure. Differences between the grain sizes and voiding effects can clearly be observed in the images.

TABLE I
PORCELAIN POWDER GRAIN SIZE ANALYSIS

Grain Size Measurement (µm)	Incisal (I)	B1	C4
Maximum Grain Size	30	33	12
Average Grain Size	16	14	7

Maximum and average grain sizes quantified in the 3 porcelain powder samples.

however difficulties in distinguishing between the surface grains and voids meant that this approach was unsuccessful. A manual void size analysis was instead implemented which identified that the largest number and most dense distribution of voids was present in the C4 shade. The maximum void size in the C4 porcelain was found to be 16.6 µm in diameter which was 1.5 times the size of the largest void the B1 shade at 11.2 µm.

B. Energy Dispersive Spectroscopy

Prior to the analytical assessment of the EDS results, a critical examination of the elements detected in each region was performed. The EDS analysis of the porcelain powders demonstrated significant amounts of carbon within the examined region. This element was found to be primarily associated with the carbon tab used to hold the powder in place and was therefore removed from the comparisons which follow. High concentrations of zirconium, gold and palladium were observed in the sintered samples; these were found to be the influence of the YPSZ discs and the conductive coating and were therefore also discounted. Unrepresentatively large variations were also observed in the weight % of oxygen across all of the samples. The elemental maps of each specimen revealed that this was again primarily due to the influence of different backing materials, and that this was not representative of the porcelain samples.

Following the collection of EDS maps of each of the porcelain samples, average EDS spectra for each of the imaged regions were generated using the 'Analyzer' routine within AZtecEnegy. This procedure produced plots plot of counts per second per electron volt (cps/eV) against detected energy (in keV) as shown in Fig. 2. The average elemental weight percentage of each of the elements was then calculated from these profiles, along with the standard deviations of each value.

Approximately uniform amounts (within the 95% confidence intervals of each value) of titanium, iron, zinc and strontium were observed in all samples at concentrations of 1.4, 0.08, 4.1 and 3.1 weight % respectively. The low concentrations associated with these elements also meant that no clear trends could be determined from the spatially resolved EDS maps.

TABLE II
SINTERED PORCELAIN SURFACE GRAIN SIZE ANALYSIS

Grain Size Measurement	Incisal (I)	B1	C4
Maximum Grain Size (µm)	5.2	17	25
Average Grain Size (µm)	1.5	2.5	5.3
Total Grain Area (µm²)	550	8,700	6,700

Total grain area, maximum and average grain sizes, quantified on the surface of the three sintered porcelain samples.
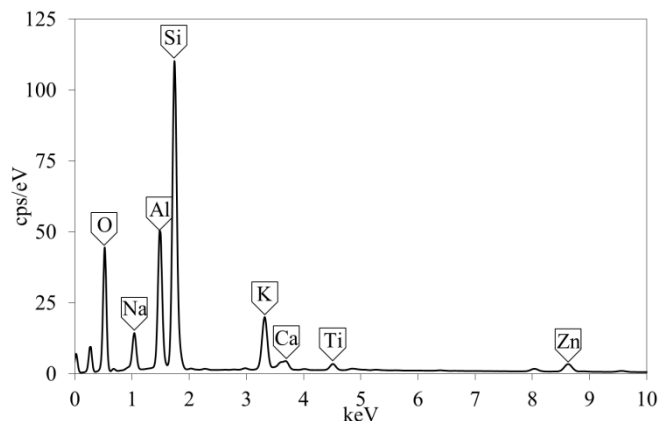

Fig. 2. Generated spectrum of counts per second per electron volt (cps/eV) against incident X-ray energy (keV) of the Incisal porcelain sample. This spectrum is an average response of the entire imaged region and the principle peaks have been annotated with their associated elements.

1) Powder Samples

The EDS analysis of the powder samples revealed distinct variations in the elemental compositions of sodium, aluminum, silicon, potassium and calcium, as shown in Fig. 3. The Incisal powder composition shows an increased concentration of aluminum compared to the shaded porcelains but a decreased concentration compared to the other four elements. In contrast, the B1 porcelain demonstrates a smaller aluminum weight % but increased levels of the other four elements. The C4 shade shows intermediate values for all of the five elements.

The large surface roughness associated with the porcelain samples meant that X-ray shadowing was observed across all of the elemental maps, this lead to regions of low elemental density across all elements. Despite this effect, examination of the unaffected regions revealed a uniform dispersal of sodium, aluminum and silicon.

In contrast to this behavior, concentrated grain like regions were observed in the calcium and potassium EDS maps in both the Incisal (I) and B1 samples as shown in Fig. 4. The high weight % of the grains could clearly be observed above the X-ray shadowing effects (as highlighted by markers in Fig. 4) and these regions were determined to have diameters in the range $1.7 - 7.4$ µm.

1) Sintered Samples

EDS analysis of the sintered samples revealed clear similarities with the average weight % of the powdered elemental specimens as shown in Fig. 5. The Incisal porcelain was again found to have the highest concentration of aluminum and the smallest concentrations of sodium,
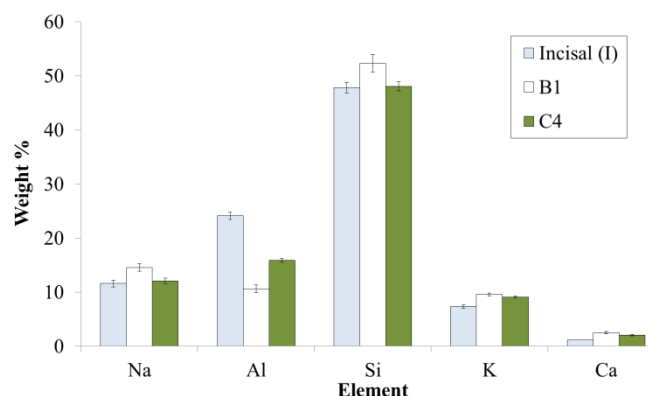

Fig. 3. Elemental weight percent of the five main elements within the powdered porcelain samples. The 95% confidence intervals have been included to demonstrate the high levels of confidence on these figures.
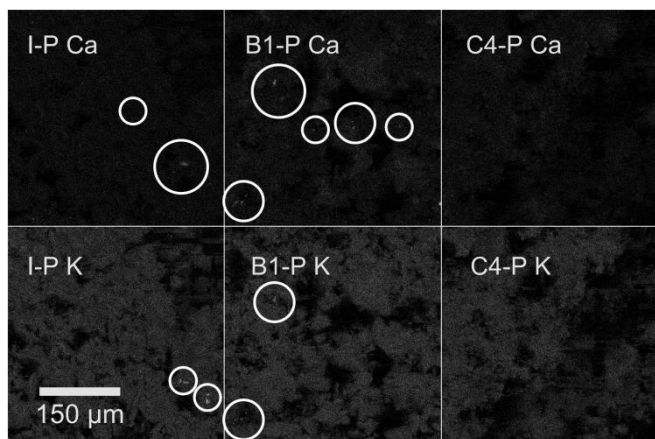
Fig. 4. Elemental weight % maps of calcium (Ca) and potassium (K) in the powered (P) Incisal (I), B1 and C4 samples. The X-ray shadowing effect can clearly be observed in the potassium images and the high elemental concentration grains have been highlighted in the Incisal and B1 specimens.

potassium and calcium. The B1 sintered porcelain showed the same reduced concentration of aluminum and an increased weight % in the other four elements. However, despite these similarities, all values showed a decrease or increase in average weight percent compared to their powder compositions. The largest change in composition was in the B1 aluminum content, which showed an apparent increase of 12.7%.

In order to quantify the impact sintering on the average elemental weight percentage of each of the five main elements, a plot of the change in weight % for each element was produced as shown in Fig. 6. It can be seen the apparent weight percentage of silicon and potassium have decreased during sintering. In contrast to this behavior an increase in sodium and aluminum weight % has been observed. Calcium has demonstrated both elemental increases and decreases in weight %, resulting in an average decrease of approximately 1%. Examination of the average change in weight percent shows that the variation in the Incisal porcelain is much smaller than for the other two shaded specimens.

The gauge volume of EDS is dependent upon both the incident angle and energy of the incoming electron beam as well as the atomic weight of the elements under consideration [13]. Taking into account the 30keV incident electron voltage, the 90° incident angle and the elemental composition of porcelain, a maximum gauge depth of 20 µm is expected in this study. For this reason these EDS results are representative of surface effects and near-surface particles previously identified through SEM imaging.
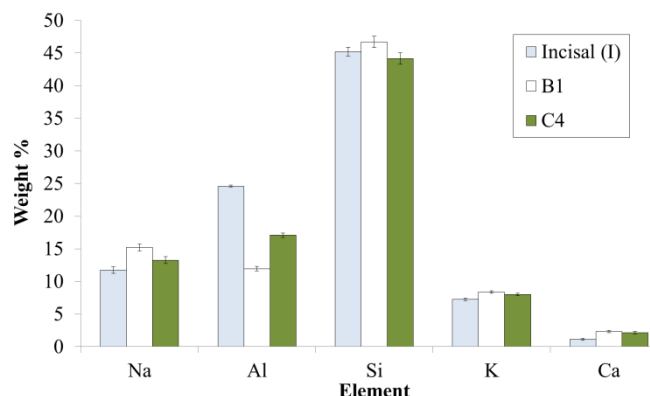

Fig. 5. Elemental weight percent of the five main elements within the sintered porcelain samples. The 95% confidence intervals have been included to demonstrate the high levels of confidence on these figures.
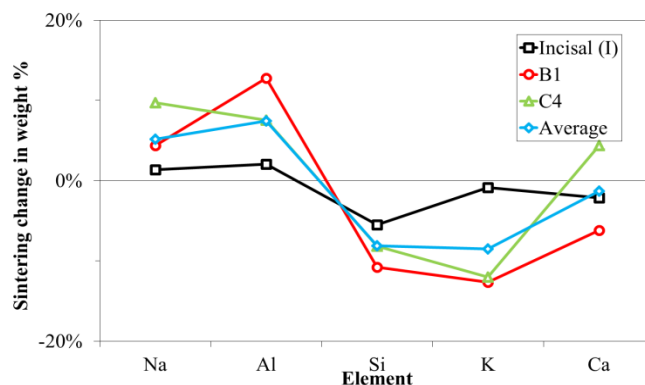

Fig. 6. Elemental weight % change of the five main elements between the powdered and sintered specimens, for all three porcelain types. An average weight percentage has also been included for comparison.

Insight into the impact of particles on the EDS results is provided by the elemental maps of the five main elements, as shown in Fig. 7. These figures demonstrate that the particles typically have higher concentrations of sodium, aluminum and calcium than the substrate material. The increased concentration of these elements results in nominal decreases in the concentration of silicon and potassium which are demonstrated by the darker regions within these elemental maps. This behavior is mirrored in the changes in average elemental composition previously highlighted.
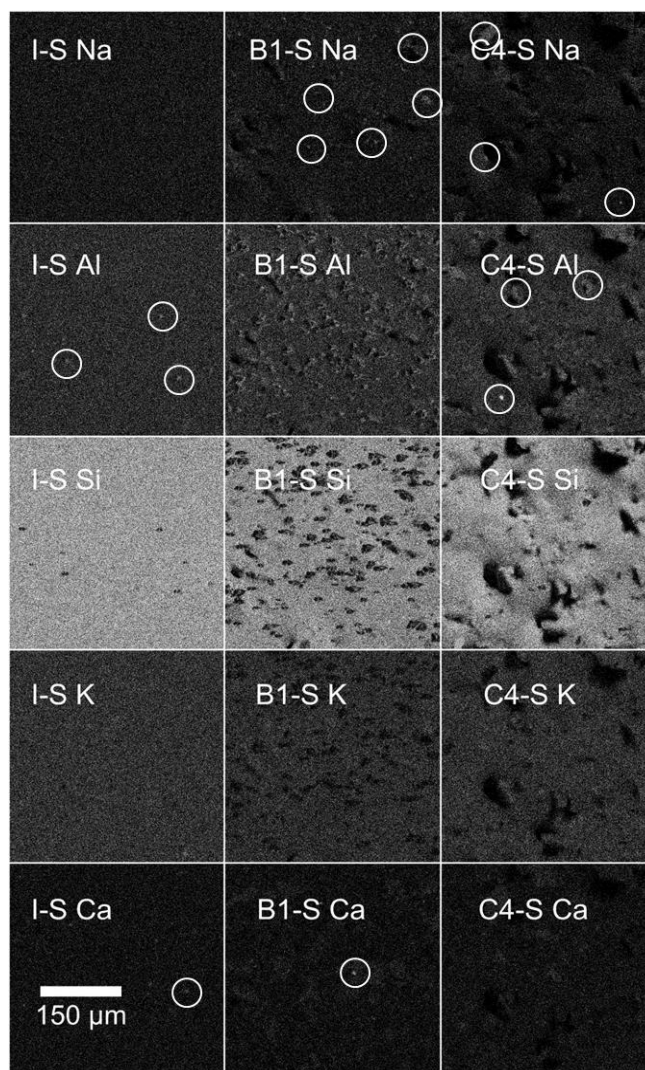

Fig. 7. Elemental weight % maps of sodium (Na), aluminum (Al), silicon (Si), potassium (K) and calcium (Ca) in the sintered (S) Incisal (I), B1 and C4 samples. The location of high concentration grains of Na, Al and Ca have been highlighted. The associated reduction in Si and K weight % can be observed in the darker regions of these maps.

As quantified in the SEM grain size analysis, a larger number of grains are present on the B1 and C4 sintered surfaces. The increased numbers of these grains is clearly demonstrated in the EDS maps of the sintered samples and therefore has a greater influence on the average weight % in these two porcelains. This result is highly consistent with the increased elemental changes observed in the B1 and C4 porcelains, as shown in Fig. 6.

IV. Discussion

The combination of SEM imaging and EDS mapping in this study has revealed clear differences in grain size and elemental composition between the Incisal (I), B1 and C4 porcelain powders. These differences form the basis of the varying colors and mechanical properties necessary to build up effective and reliable dental prosthesis. For this reason, the exact material compositions form part of the intellectual property of the manufacturer and only approximate ranges of oxide concentrations of these porcelains have been released [14]. The average elemental weights of this study fall within the bounds of the manufacturer estimates, however care must be taken when considering the absolute magnitudes presented by EDS analysis, particularly for the atoms of low atomic mass (Na, Al and Si) considered in this study [15]. The consistency of the elemental weight % values in the differing specimens and clear trends observed in these results does however suggest that the relative variations are likely to be reliable.

IPS e.max$^{®}$ Ceram is a glass ceramic which contains crystals of fluroapatite ($Ca_5(PO_4)_3F$) [14] and these grains are clearly demonstrated by the high concentration calcium grains observed in the Incisal and B1 samples powder samples (Fig. 4). Despite observing these distinctions in calcium content, neither fluorine nor phosphorous were identified in the EDS analysis. In the case of fluorine this lack of detection is based on the low atomic weight (18.99 u) of this element and the inherent insensitivity of EDS to these elements. The lack of phosphorous detection, was based on the overlap observed between the phosphorous K-alpha peak (2.013keV) and the zirconium L-alpha peak (2.042keV) [16]. The interference between these two peaks and the exclusion of zirconium (due to the varying influence of backing materials) meant that effective EDS analysis of this phosphorous was not possible.

In contrast to many dental porcelains, IPS e.max$^{®}$ Ceram does not contain potassium feldspar ($KAlSi_3O_8$) [14] and therefore the potassium rich grains observed in the EDS study are not representative of this compound. None of other elements considered in this study showed correlation with these grains, suggesting that the high potassium concentration grains are most likely to be K_2O.

A review of the literature on dental porcelain powder grain size analysis reveals a comprehensive study of unshaded porcelains by Sınmazışık et. al [8]. They observed bi-modal distributions within a range of commercially available porcelains and average grain sizes in the range $14.6 - 23.3\,\mu m$. The use of bi-modal grain distributions has previously been shown to lead to reduced sintering shrinkage [17] and therefore forms part of the manufacturing process of many commercially available dental porcelains.

In this study, the unshaded Incisal porcelain demonstrates an average grain size of 16 μm which is within the range of the literature values previously identified. However no comparable literature values could be identified for the smaller grains sizes observed in the B1 and C4 shaded porcelains. It is believed therefore that these differences present new insight into the powder structure of these shaded porcelain compositions.

The limited grain numbers identified in this study meant that no clear conclusions could be drawn on the modal grain size distributions of the porcelains. The presence of very large grains (33 μm) and moderate average grain sizes (14 μm) in the B1 porcelain, does however suggest that this behavior may be indicative of this bi-modal distribution.

Following the implementation of the manufacturer's recommended sintering regime, clear differences between the Incisal and shaded porcelain surfaces could be observed. The sintering applied to the unshaded porcelain appears to have induced a much more uniform veneer in terms of surface topology and elemental distribution. In contrast to this behavior, incomplete sintering appears to have occurred in both of the shaded veneers as demonstrated by the surface voiding and the element rich grains on the surface.

Similar elementally distinct grain like regions of fluroapatite have previously been observed in the melt pool of sintered dental porcelains [8, 18]. Based on this insight, and in combination with the calcium rich regions observed in this study, it is believed that a similar response has been observed here.

Incomplete sintering and the porosity associated with this phenomena are known to increase the likelihood of cracking [9] and to reduce component lifetimes [10] in dental prosthesis. Therefore, based on the results of this study, early lifetime failure would likely be expected in B1 or C4 shaded porcelain which has been exposed to a single sintering cycle.

Despite this result, shading porcelain is only ever used as an intermediate compound in the buildup of porcelain copings and is therefore exposed to multiple sintering cycles during manufacture. This repeated sintering has previously been shown to increase the density and reduce porosity in IPS e.max$^{®}$ Ceram and the resulting microstructure has been found to be both harder and tougher than single cycled samples [19, 20]. For this reason, and taking into account the lack of documented failures in these two porcelain shades, these further sintering cycles likely increase the porcelain densities and improve their mechanical responses, in practical use.

V. Conclusions

The combination of SEM imaging and EDS mapping in this study has revealed distinct differences between the Incisal (I), B1 and C4 IPS e.max® Ceram powdered porcelains. The different functions associated with these three types of porcelain have resulted in not only different average elemental compositions but also variations in the maximum and average grain sizes within each of the powders.

The impact of sintering was also shown to influence the resulting microstructure of each of the three porcelain powders in different ways. The Incisal (I) porcelain revealed a highly uniform surface with limited evidence for surface graining and no evidence of porosity. The B1 porcelain demonstrated large numbers of aluminum, sodium and calcium rich grains, along with small amounts of surface porosity. In contrast to this, the C4 porcelain showed smaller numbers of larger aluminum, sodium and calcium rich

grains on the sintered surface and the porosity was found to be much more prominent, both in terms of numbers of pores and maximum pore size.

Despite the limited number of samples studied here, the sensitivity of the sintered microstructure to both the porcelain powder and sintering conditions has been revealed in this study. This high level of sensitivity may explain some of the stochastic YPSZ-porcelain interface failures observed in practice and suggests that further more detailed studies may be necessary to fully capture the influence of these variables and thereby improve prosthesis implant reliability.

REFERENCES

[1] A. J. Raigrodski, M. B. Hillstead, G. K. Meng, and K. H. Chung, "Survival and complications of zirconia-based fixed dental prostheses: A systematic review," in *The Journal of prosthetic dentistry,* vol. 107, no. 3, pp. 170-177, 2012.

[2] I. Denry and J. A. Holloway, "Ceramics for Dental Applications: A Review," in *Materials,* vol. 3, no. 1, pp. 351-368, 2010.

[3] M. J. Kim, et al., "Wear evaluation of the human enamel opposing different Y-TZP dental ceramics and other porcelains," in *Journal of Dentistry,* vol. 40, no. 11, pp. 979-988, 2012.

[4] J. Schmitt, et al., "Zirconia Posterior Fixed Partial Dentures: A Prospective Clinical 3-year Follow-up," in *International Journal of Prosthodontics,* vol. 22, no. 6, pp. 597-603, 2009.

[5] A. K. Mainjot, G. S. Schajer, A. J. Vanheusden, and M. J. Sadoun, "Influence of zirconia framework thickness on residual stress profile in veneering ceramic: Measurement by hole-drilling," in *Dental Materials,* vol. 28, no. 4, pp. 378-384, 2012.

[6] A. J. G. Lunt, et al., "A Correlative Microscopy Study of the Zirconia - Porcelain Interface in Dental Prostheses: TEM, EDS and Micro-pillar Compression," in *Surface and Coatings Technology,* submitted for publication

[7] A. Pelaez-Vargas, et al., "The effect of slurry preparation methods on biaxial flexural strength of dental porcelain," in *The Journal of prosthetic dentistry,* vol. 105, no. 5, pp. 308-314, 2011.

[8] G. Sınmazışık and M. L. Öveçoğlu, "Physical properties and microstructural characterization of dental porcelains mixed with distilled water and modeling liquid," in *Dental Materials,* vol. 22, no. 8, pp. 735-745, 2006.

[9] X. Wu, M. Nakagawa, and F. Teraoka, "Failure morphology of all-ceramic prostheses," in *Dental materials journal,* vol. 31, no. 3 pp. 494-498, 2012.

[10] M. Borba, et al., "Effect of the microstructure on the lifetime of dental ceramics," in *Dental Materials,* vol. 27, no. 7, pp. 710-721, 2011.

[11] (2015, March 21). IPS e.max Ceram Instructions for Use. [Online]. Available: http://downloads.ivoclarvivadent.com/zoolu-website/media/document/1264/IPS+e-max+Ceram

[12] M. D. Abràmoff, P. J. Magalhães, and S. J. Ram, "Image processing with ImageJ," in *Biophotonics international,* vol. 11, no. 7, pp.36-43, 2004.

[13] K. Tsuji, J. Injuk, and R. Van Grieken, *X-Ray Spectrometry: Recent Technological Advances.* New York, NY: Wiley, 2005, pp. 412-448.

[14] (2015, March 21). IPS e.max® Ceram Scientific Documentation [Online] Available: http://www.roedentallab.com/downloads/emaxceramicdata.pdf.

[15] D. Bell and A. Garratt-Reed, *Energy Dispersive X-ray Analysis in the Electron Microscope.* London, UK: Taylor & Francis, 2003, pp. 92.

[16] J. W. Robinson, *Practical Handbook of Spectroscopy.* London, UK: Taylor & Francis, 1991, pp. 740.

[17] S. T. Rasmussen, W. Ngaji-Okumu, K. Boenke, and W. J. O'Brien, "Optimum particle size distribution for reduced sintering shrinkage of a dental porcelain," in *Dental Materials,* vol. 13, no. 1, pp.43-50, 1997.

[18] E. Kontonasaki, et al., "Microstructural characterization and comparative evaluation of physical, mechanical and biological properties of three ceramics for metal–ceramic restorations," in *Dental Materials,* vol. 24, no. 10, pp.1362-1373, 2008.

[19] X. Tang, T. Nakamura, H. Usami, K. Wakabayashi, and H. Yatani, "Effects of multiple firings on the mechanical properties and microstructure of veneering ceramics for zirconia frameworks," in *Journal of Dentistry,* vol. 40, no. 5, pp.372-380, 2012.

[20] K. C. Cheung and B. W. Darvell, "Sintering of dental porcelain: effect of time and temperature on appearance and porosity," in *Dental Materials,* vol. 18, no. 2, pp.163-173, 2002.